47th AIAA Aerospace Sciences Meeting Including The New Horizons Forum and Aerospace Exposition
5 - 8 January 2009, Orlando, Florida

AIAA 2009-459

Low Magnetic Reynolds Number Hypersonic MHD Flow Using High Order WENO Schemes

Jaejin Lee*, Manuel A. Huerta†, and Gecheng Zha‡
University of Miami
Coral Gables, Florida 33124

In this paper we incorporate a low magnetic Reynolds number MHD model to a high order CFD algorithm with WENO and a low diffusion scheme for 3D Navier-Stokes equations. We present results for hypersonic laminar flows around a flat plate and around a blunt body, with different strengths of magnetic fields, to demonstrate the methodology. More simulations, including turbulence, are in progress and will be reported in the final paper.

I. Introduction

Hypersonic vehicles generate shocks that can heat the air sufficiently to partially ionize the air and create an electrically conducting plasma that can be studied using the equations of single fluid magnetohydrodynamics (MHD), also called magnetofluiddynamics (MFD). Introducing strong applied magnetic and electric fields into the flow could have beneficial effects such as reducing heat damage, providing a sort of MHD parachute, and generating electric power or thrust in the vehicle. Among the many authors that have done numerical simulations of hypersonic MHD flows we mention here Bityurin, Lineberry, Potebnia, et. al.,[1] Bityurin and Bocharov,[2] Bityurin, Zeigarnik and Kuranov,[3] Fujino, Kondo and Ishikawa,[4] MacCormack,[5] and Hoffmann, Damevin, and Dietiker.[6] To simulate hypersonic flow with MHD it is essential to have a flow solver that can capture shock waves and turbulence accurately. Recently a low diffusion E-CUSP (LDE) scheme with a fifth order WENO scheme was developed to resolve flow fields with shock discontinuities. The purpose of this paper is to incorporate the low magnetic Reynolds number MHD model to the CFD algorithm so that it can be used to simulate hypersonic flows with MHD effects. Realistic flows are turbulent, but in this paper we only show results for laminar low. In the final paper we will include turbulence.

II. The MHD Model

Single-fluid magnetohydrodynamics (MHD) describes an electrically conducting but electrically neutral fluid of density ρ, velocity $\mathbf{u}$, pressure p, energy per unit mass e, viscosity tensor $\bar{\bar{\tau}}$, and heat flux vector $\mathbf{q}$. The electrical quantities are the magnetic field $\mathbf{B}$, the electric field $\mathbf{E}$, the current density $\mathbf{J}$, and the electrical conductivity σ, which may be a scalar or a tensor, depending on the model. In principle σ should be calculated from an air chemistry model, such as in Ref. [5], but in this paper we assume that σ is given, and we do not discuss the air chemistry. The plasma is taken to obey Ohm's law

$$\mathbf{J} = \sigma(\mathbf{E} + \mathbf{u} \times \mathbf{B}). \tag{1}$$

The magnetic field is advanced in time using Faraday's law

$$\frac{\partial \mathbf{B}}{\partial t} = -\nabla \times \mathbf{E}. \tag{2}$$

* Graduate Student, Department of Physics
† Professor, Department of Physics, AIAA Member
‡ Associate Professor, Department of Mechanical and Aerospace Engineering, Senior AIAA Member

The Ampère-Maxwell equation, which could be used to advance $\mathbf{E}$ is

$$\mu_0\epsilon_0\frac{\partial \mathbf{E}}{\partial t} = \nabla \times \mathbf{B} - \mu_0\mathbf{J}. \tag{3}$$

However, MHD describes low frequency phenomena, in which the conduction current is much greater than the displacement current, that is,

$$\mathbf{J} \gg \epsilon_0\frac{\partial \mathbf{E}}{\partial t}. \tag{4}$$

The displacement current is therefore neglected and we use the pre-Maxwell equation

$$\mu_0\mathbf{J} = \nabla \times \mathbf{B}, \tag{5}$$

which gives $\mathbf{J}$ in terms of $\mathbf{B}$. This means that $\mathbf{E}$ is not advanced in time, but is obtained in terms of $\mathbf{B}$ using Eqs. [1] and [5]. As a consequence of this, MHD cannot describe the usual type of high frequency electromagnetic waves. However, MHD does describe three interesting types of waves known as the Alfvén wave and the fast and slow magneto-acoustic waves. Therefore $\mathbf{E}$ can be eliminated from Eq.(2) and we rewrite it as

$$\frac{\partial \mathbf{B}}{\partial t} = -\nabla \times \big(\frac{\mathbf{J}}{\sigma} - \mathbf{u} \times \mathbf{B}\big) = \nabla \times (\mathbf{u} \times \mathbf{B}) + \frac{1}{\mu_0\sigma}\nabla^2\mathbf{B}, \tag{6}$$

which is the equation that advances $\mathbf{B}$ in time, and can be written in conservation form as

$$\frac{\partial \mathbf{B}}{\partial t} + \nabla \cdot (\mathbf{u} \otimes \mathbf{B} - \mathbf{B} \otimes \mathbf{u}) = \frac{1}{\mu_0\sigma}\nabla^2\mathbf{B}. \tag{7}$$

The fluid quantities $\rho, \mathbf{u}$, and e are advanced in time using the usual conservation of mass,

$$\frac{\partial \rho}{\partial t} + \nabla \cdot (\rho\mathbf{u}) = 0, \tag{8}$$

conservation of momentum,

$$\frac{\partial (\rho\mathbf{u})}{\partial t} + \nabla \cdot (\rho\mathbf{u} \otimes \mathbf{u}) = -\nabla p + \nabla \cdot \bar{\bar{\tau}} + \mathbf{J} \times \mathbf{B}, \tag{9}$$

which now includes the magnetic force density $\mathbf{J} \times \mathbf{B}$, and finally e is advanced with the equation of conservation of energy,

$$\frac{\partial}{\partial t}\big(\rho(e + \frac{1}{2}u^2)\big) + \nabla \cdot \big(\rho\big(e + \frac{1}{2}u^2 + p\big)\mathbf{u}\big) = -\nabla \cdot \mathbf{q} + \nabla \cdot (\bar{\bar{\tau}} \cdot \mathbf{u}) + \mathbf{E} \cdot \mathbf{J}. \tag{10}$$

This equation is rewritten using Eq. [1] as

$$\frac{\partial}{\partial t}\big(\rho(e + \frac{1}{2}u^2)\big) + \nabla \cdot \big(\rho\big(e + \frac{1}{2}u^2 + p\big)\mathbf{u}\big) = -\nabla \cdot \mathbf{q} + \nabla \cdot (\bar{\bar{\tau}} \cdot \mathbf{u}) + \frac{J^2}{\sigma} + (\mathbf{J} \times \mathbf{B}) \cdot \mathbf{u}. \tag{11}$$

Another form of Eq. [10] is obtained by using Eqs. [2] and [5],

$$\frac{\partial}{\partial t}\big(\rho(e + \frac{1}{2}u^2) + \frac{B^2}{2\mu_0}\big) + \nabla \cdot \left(\rho(e + \frac{1}{2}u^2)\mathbf{u} + p\mathbf{u} + \frac{\mathbf{E} \times \mathbf{B}}{\mu_0}\right) = -\nabla \cdot \mathbf{q} + \nabla \cdot (\bar{\bar{\tau}} \cdot \mathbf{u}), \tag{12}$$

from which we may eliminate $\mathbf{E}$ using Eq. [1], and we get

$$\frac{\partial}{\partial t}(\rho e_t) + \nabla \cdot \left(\rho e_t\mathbf{u} + \big(p + \frac{B^2}{2\mu_0}\big)\mathbf{u} - \frac{\mathbf{B}\mathbf{B} \cdot \mathbf{u}}{\mu_0} + \frac{\mathbf{J} \times \mathbf{B}}{\mu_0\sigma}\right) = -\nabla \cdot \mathbf{q} + \nabla \cdot (\bar{\bar{\tau}} \cdot \mathbf{u}), \tag{13}$$

where e_t is the total energy density.

$$e_t = e + \frac{1}{2}u^2 + \frac{B^2}{2\mu_0}. \tag{14}$$

In Eqs. [9], [11], and [13] $\mathbf{J}$ can be eliminated using Eqs. [1] or [5] as the case may be. The system is closed by giving appropriate expressions for $e, \bar{\bar{\tau}}, \mathbf{q}$, and σ in terms of the other quantities. Typically a simple form for e is used,

$$e = \frac{p}{(\gamma - 1)\rho}, \quad \text{where} \quad \gamma = 1.4 \quad \text{for air.} \tag{15}$$

III. The Full MHD Model and the Low Magnetic Reynolds Number Approximation

The full MHD model presented in Section II advances in time the eight-dimensional flux vector $[\rho, \rho u, \rho v, \rho w, \rho e_t, B_x, B_y, B_z]$, where u, v, and w are the x, y, and z components of $\mathbf{u}$, using Eqs. [8], [9], [13], and [7] in conservation form. The only electrical quantities that appear in the equations are $\mathbf{B}, \sigma$, and μ_0, although the presence of $\mathbf{E}$ is felt in the boundary conditions. Several authors have treated the full 8-dimensional problem. For example, a nozzle problem with a generator section to extract power from the incoming flow, and an accelerator section to produce thrust, using a tensor conductivity was treated in Ref. [5]. Ref. [6] also used the full 8-dimensional MHD model to treat flows around a flat plate and around a blunt body with zero electric field. The full MHD 8-dimensional problem is conceptually clear, because the magnetic and electric fields, $\mathbf{B}$ and $\mathbf{E}$ are calculated. In this case $\mathbf{J}$ is obtained from Eq. [5], and $\mathbf{E}$ is obtained from Eq. [1], although the boundary conditions have an important effect on what $\mathbf{E}$ must be. The numerical simulations are complicated, however.

The vehicle may have an electrically insulating surface and carry a magnet that applies a strong magnetic field $\mathbf{B}_a$ to the flow if the intention is to reduce surface heating and increase the drag force in a sort of MHD parachute. The vehicle may also have conductors on its surface, which change the boundary conditions, to try to generate electrical power by extracting energy from the flow. The vehicle might also have a source of $\mathcal{E}$mf, $\mathcal{E}_a$, and apply a strong electric field $\mathbf{E}_a$, such as in a nozzle to produce MHD thrust. The total magnetic and electric fields in the plasma, $\mathbf{B} = \mathbf{B}_a + \mathbf{B}_i$ and $\mathbf{E} = \mathbf{E}_a + \mathbf{E}_i$, are the sum of the applied and induced fields. However, the ionized air produced in the hypersonic flow is a poor electrical conductor. Therefore the electrical current $\mathbf{J}$ induced in the plasma is small, and the magnetic $\mathbf{B}_i$ generated by the plasma current is much smaller than the applied field. This allows the use of a low magnetic Reynolds number approximation. When expressed in dimensionless variables, the electrical conductivity σ enters the problem via the magnetic Reynolds number

$$R_m = \mu_0 \sigma U_{ref} L_{ref}, \tag{16}$$

where U_{ref} and L_{ref} are appropriate reference values of speed and length in the problem. When R_m is small it is possible to treat the problem in a low R_m approximation, which neglects the fields $\mathbf{B}_i$ and $\mathbf{E}_i$ induced by the plasma. In this model only the five fluid quantities in the five-dimensional flux vector $[\rho, \rho u, \rho v, \rho w, \rho e]$ need to be advanced in time using Eqs.[8], [9], and [11], with MHD source terms proportional to $\mathbf{J}$. Refs. [1] - [4] used the low R_m approximation to study interesting effects, such as the MHD parachute and MHD power generation. MacCormack[7] showed that the full MHD solution agrees with the low R_m solution for flow in a thrust producing nozzle for $R_m = 0.17$. Damevin and Hoffmann[8] compared the full MHD solution including air chemistry with the low R_m approximation in flows over a hemisphere and a cylinder. Khan, Hoffmann and Dietiker[9] used the full MHD model to treat flows with zero electric field around a flat plate and a blunt body and tested for agreement between the solutions of the full MHD model and the low R_m approximation. They obtained good agreement for values of $R_m < 0.125$.

To understand the validity of the low R_m approximation we can think in terms of a sort of singular expansion in the small parameter R_m that would allow one to calculate the $O(R_m)$ quantities that are neglected in the low R_m approximation. From Eq. [1] we see that the current is proportional to σ, so $\mathbf{J}$ is $O(R_m)$, and from Eq. [5] we see that $\mathbf{B}_i$ is also $O(R_m)$.

Therefore the source terms in Eqs. [8], [9], and [11] are accurately kept through order $O(R_m)$ by writing

$$\mathbf{J} \times \mathbf{B} \approx \mathbf{J} \times \mathbf{B}_a, \tag{17}$$

and taking

$$\mathbf{J} \approx \sigma(\mathbf{E}_a + \mathbf{u} \times \mathbf{B}_a). \tag{18}$$

One would not use Eq. [5] to get $\mathbf{J}$ from $\mathbf{B}_i$, as in the full MHD model, but rather, in a kind of reversal that is typical of singular approximations, in the low R_m approximation $\mathbf{B}_i$, if needed, could be calculated from $\mathbf{J}$ using Eq. [5]. Therefore the induced magnetic field would be obtained from the ususal equation of magnetostatics,

$$\mathbf{B}_i(\mathbf{r}) = \frac{\mu_0}{4\pi} \int \frac{\mathbf{J} \times (\mathbf{r} - \mathbf{r}')}{|\mathbf{r} - \mathbf{r}'|^3} dV' = \frac{\mu_0 \sigma}{4\pi} \int \frac{(\mathbf{E}_a + \mathbf{u} \times \mathbf{B}_a) \times (\mathbf{r} - \mathbf{r}')}{|\mathbf{r} - \mathbf{r}'|^3} \, dV, \tag{19}$$

but there would still remain the problem of determining what is the electric field $\mathbf{E} = \mathbf{E_a} + \mathbf{E}_i$. Since $\nabla \cdot \mathbf{J} = 0$, we have

$$\nabla \cdot \mathbf{E} = \nabla \cdot \mathbf{E}_i = -\nabla \cdot (\mathbf{u} \times \mathbf{B}_a). \tag{20}$$

For example in the two dimensional problems where $u_z = B_z = 0$ and $\partial/\partial z = 0$, or where $u_\phi = B_\phi = 0$ and $\partial/\partial\phi = 0$, $\nabla \cdot \mathbf{E} = 0$. Then the curl of $\mathbf{E}_i$ is obtained from the time derivative of Eq. [19]. The boundary conditions are important in finding the electric field. For example, in the problem of steady flow past a flat plate treated in Khan,[9] they have a current in the ignorable direction $J_z(x, y)$, and the total electric field to order $O(R_m^0)$ is taken as zero. The electric field being zero implies that the current has a zero resistance return path located outside the plasma. If the return path were a passive resistance R, as might be the case in an MHD generator, then the induced electric field would be entirely due to the boundary conditions and would be a constant of order $O(R_m)$, $\mathbf{E} = E_{i_z}(BC)\mathbf{z} = -\frac{iR}{2L_z}\mathbf{z}$. Here the total current i is

$$i = \int Jzdxdy \quad \text{of} \quad O(R_m). \tag{21}$$

If the return path not only had had a resistance R, but also an applied $\mathcal{E}_a$ acting in the opposite direction of $(\mathbf{u} \times \mathbf{B})_z$, then the electric field in the plasma would be

$$\mathbf{E} = -\frac{\mathcal{E}_a + iR}{L_z}\hat{\mathbf{z}}. \tag{22}$$

In an MHD accelerator one would make $\mathcal{E}_a/L_z$ larger in magnitude than $|(\mathbf{u}\times\mathbf{B})_z|$ and opposite in direction. If the return path had infinite resistance, an open circuit, then $J_z = 0$ everywhere, and one would have that $\mathbf{E} = -\mathbf{u} \times \mathbf{B}_a$, so one could say that $\mathbf{E}_i$ would be $O(R_m^0)$. This of course would not be a case of interest because $\mathbf{J} = 0$. In the problem with cylindrical symmetry mentioned above, the applied field would typically have r and z components

The above discussion is not quite the same as doing a formal power series expansion in R_m because in the low R_m approximation the fluid quantities $\mathbf{u}, \rho, p$, etc. are

$$\mathbf{u} = \mathbf{u}^{(0)} + R_m\mathbf{u}^{(1)}, \quad \rho = \rho^{(0)} + R_m\rho^{(1)} \quad p = p^{(0)} + R_m p^{(1)}. \tag{23}$$

The order $O(R_m)$ terms are kept in the fluid quantities in order to see the plasma effects upon things like the location and strength of shocks.

IV. The Governing Equations of a Three-dimensional Low R_m Approximation

We use a generalized coordinate system

$$\xi(x, y, z), \quad \eta(x, y, z), \quad \zeta(x, y, z) \quad \text{with} \quad J = \frac{\partial(\xi, \eta, \zeta)}{\partial(x, y, z)}, \tag{24}$$

where J is the Jacobian determinant of the transformation of variables. We use the E-CUSP (energy-convective-upstream-split-pressure) scheme developed by Zha, Shen, and Wang.[10] The governing equations Eqs.[8], [9], and [11], coupled with the Baldwin - Lomax turbulence model are as follows.

$$\frac{\partial Q}{\partial t} + \frac{\partial \mathbf{E}}{\partial \xi} + \frac{\partial \mathbf{F}}{\partial \eta} + \frac{\partial \mathbf{G}}{\partial \zeta} = \frac{1}{Re}\left(\frac{\partial \mathbf{R}}{\partial \xi} + \frac{\partial \mathbf{S}}{\partial \eta} + \frac{\partial \mathbf{T}}{\partial \zeta} + \mathbf{D}\right) + \mathbf{S}_{MHD}. \tag{25}$$

The flux vector is

$$Q = \frac{1}{J}[\ \rho, \quad \rho u, \quad \rho v, \quad \rho w, \quad \rho e\ ]^T \tag{26}$$

where u, v and w are the x, y and z components of the fluid velocity. The vector $\mathbf{S}_{MHD}$ contains the MHD source terms,

$$\mathbf{S}_{MHD} = \frac{1}{J}[\ 0, \quad (\mathbf{J} \times \mathbf{B}_a)_x, \quad (\mathbf{J} \times \mathbf{B}_a)_y, \quad (\mathbf{J} \times \mathbf{B}_a)_z, \quad \mathbf{E} \cdot \mathbf{J}\ ]^T \tag{27}$$

where

$$\mathbf{J} = \sigma(\mathbf{E} + \mathbf{u} \times \mathbf{B}_a), \tag{28}$$

and $\mathbf{E}$ is determined using the boundary conditions. Typically, to lowest order in R_m,

$$\mathbf{E} = \mathbf{E}_a, \quad \text{and} \quad \mathbf{J} = \sigma(\mathbf{E}_a + \mathbf{u} \times \mathbf{B}_a). \tag{29}$$

We note that $\mathbf{E} \cdot \mathbf{J}$ can be rewritten as

$$\mathbf{E} \cdot \mathbf{J} = \frac{\mathbf{J} \cdot \mathbf{J}}{\sigma} + (\mathbf{J} \times \mathbf{B}_a) \cdot \mathbf{u}, \tag{30}$$

We introduce the vectors $\mathbf{l}$, $\mathbf{m}$, $\mathbf{n}$. These are the normal vectors on ξ, η, ζ surfaces with their magnitudes equal to the elemental surface area and pointing to the directions of increasing ξ, η, ζ,

$$\mathbf{l} = \frac{\nabla\xi}{J}\Delta\eta\Delta\zeta, \ \mathbf{m} = \frac{\nabla\eta}{J}\Delta\xi\Delta\zeta, \ \mathbf{n} = \frac{\nabla\zeta}{J}\Delta\xi\Delta\eta. \tag{31}$$

l_t, m_t, n_t stand for the grid moving velocities and are defined as

$$l_t = \frac{\xi_t}{J}\Delta\eta\Delta\zeta, \ m_t = \frac{\eta_t}{J}\Delta\xi\Delta\zeta, \ n_t = \frac{\zeta_t}{J}\Delta\xi\Delta\eta \tag{32}$$

When the grid is stationary, $l_t = m_t = z_t = 0$. Since $\Delta\xi = \Delta\eta = \Delta\zeta = 1$ in the current discretization, Eqs.(31) and (32) are written as the following in the solver,

$$\mathbf{l} = \frac{\nabla\xi}{J}, \ \mathbf{m} = \frac{\nabla\eta}{J}, \ \mathbf{n} = \frac{\nabla\zeta}{J}, \tag{33}$$

and

$$l_t = \frac{\xi_t}{J}, \ m_t = \frac{\eta_t}{J}, \ n_t = \frac{\zeta_t}{J}. \tag{34}$$

The matrices $\mathbf{E}$, $\mathbf{F}$, and $\mathbf{G}$ are

$$\mathbf{E} = \begin{bmatrix} \rho U \\ \rho u U + l_x p \\ \rho v U + l_y p \\ \rho w U + l_z p \\ (\rho e + p) U - l_t p \end{bmatrix}, \ \mathbf{F} = \begin{bmatrix} \rho V \\ \rho u V + m_x p \\ \rho v V + m_y p \\ \rho w V + m_z p \\ (\rho e + p) V - m_t p \end{bmatrix}, \ \mathbf{G} = \begin{bmatrix} \rho W \\ \rho u W + n_x p \\ \rho v W + n_y p \\ \rho w W + n_z p \\ (\rho e + p) W - n_t p \end{bmatrix}. \tag{35}$$

In the equations above, U, V and W are the contravariant velocities in the ξ, η and ζ directions,

$$\begin{aligned} U &= l_t + \mathbf{l} \cdot \mathbf{V} = l_t + l_x u + l_y v + l_z w \\ V &= m_t + \mathbf{m} \cdot \mathbf{V} = m_t + m_x u + m_y v + m_z w \\ W &= n_t + \mathbf{n} \cdot \mathbf{V} = n_t + n_x u + n_y v + n_z w, \end{aligned} \tag{36}$$

where $\mathbf{V} = (u, v, w)$ is the velocity vector. The viscosity and heat conduction flux vectors $\mathbf{R}, \mathbf{S}$, and $\mathbf{T}$ are

$$\mathbf{R} = \begin{bmatrix} 0 \\ l_k\tau_{xk} \\ l_k\tau_{yk} \\ l_k\tau_{zk} \\ l_k\beta_k \end{bmatrix}, \ \mathbf{S} = \begin{bmatrix} 0 \\ m_k\tau_{xk} \\ m_k\tau_{yk} \\ m_k\tau_{zk} \\ m_k\beta_k \end{bmatrix}, \ \mathbf{T} = \begin{bmatrix} 0 \\ n_k\tau_{xk} \\ n_k\tau_{yk} \\ n_k\tau_{zk} \\ n_k\beta_k \end{bmatrix}, \tag{37}$$

where

$$\beta_k = u_i\tau_{ki} - q_k. \tag{38}$$

The shear-stress τ_{ik} and total heat flux q_k in Cartesian Coordinate can be expressed as

$$\tau_{ik} = (\mu + \mu_t)\left[\left(\frac{\partial u_i}{\partial x_k} + \frac{\partial u_k}{\partial x_i}\right) - \frac{2}{3}\delta_{ik}\frac{\partial u_j}{\partial x_j}\right] \tag{39}$$

$$q_k = -\left(\frac{\mu}{Pr} + \frac{\mu_t}{Pr_t}\right)\frac{\partial T}{\partial x_k} \tag{40}$$

where, Pr is the Prandtl number, Pr_t is the turbulent Prandtl number, μ is the molecular viscosity determined by the Sutherland law and μ_t is the turbulent viscosity determined by the Baldwin - Lomax model. In eqs.(37), (38), (39) and (40), the repeated subscripts i or k represent the coordinates x, y and z following the Einstein summation convention. Eqs.(39) and (40) are transformed to the generalized coordinate system in the computation.

The vector $\mathbf{D}$ in Eq. (25) appears when the coordinate transformation is time dependent and is given by

$$\mathbf{D} = \mathbf{U}\left[\frac{\partial J^{-1}}{\partial t} + \left(\frac{\xi_t}{J}\right)_\xi + \left(\frac{\eta_t}{J}\right)_\eta + \left(\frac{\zeta_t}{J}\right)_\zeta\right].$$

V. The Numerical Scheme

The inviscid fluxes are evaluated using the LDE scheme of Ref. [10] and the fifth order WENO scheme given below. The viscous terms are discretized using a 2nd order central differencing scheme. We compare the results with a MUSCL scheme.

V.A. The Low Diffusion E-CUSP (LDE) Scheme

The basic idea of the E-CUSP scheme is to split the inviscid flux into the convective flux E^c and the pressure flux E^p. In a generalized coordinate system, the flux $\mathbf{E}$ can be split as follows

$$\mathbf{E} = E^c + E^p = \begin{pmatrix} \rho U \\ \rho u U \\ \rho v U \\ \rho w U \\ \rho e U \end{pmatrix} + \begin{pmatrix} 0 \\ l_x p \\ l_y p \\ l_z p \\ p\overline{U} \end{pmatrix}, \tag{41}$$

where

$$\overline{U} = l_x u + l_y v + l_z w. \tag{42}$$

The convective term, E^c is evaluated following the Edward's H-CUSP (enthalpy-CUSP) LDFSS[11,12](low-diffusion-flux-splitting-scheme) ,

$$E^c = \rho U \begin{pmatrix} 1 \\ u \\ v \\ w \\ e \end{pmatrix} = \rho U f^c,\ f^c = \begin{pmatrix} 1 \\ u \\ v \\ w \\ e \end{pmatrix}. \tag{43}$$

Let

$$C = c\left(l_x^2 + l_y^2 + l_z^2\right)^{\frac{1}{2}} \tag{44}$$

where $c = \sqrt{\gamma RT}$ is the speed of sound. Then the convective flux at interface $\frac{1}{2}$ is evaluated as:

$$E^c_{\frac{1}{2}} = C_{\frac{1}{2}}\left[\rho_L C^+ f^c_L + \rho_R C^- f^c_R\right], \tag{45}$$

where, the subscripts L and R represent the left and right hand sides of the interface.

The interface speed of sound is

$$C_{\frac{1}{2}} = \frac{1}{2}\left(C_L + C_R\right). \tag{46}$$

The following relations are borrowed from Edwards LDFFS scheme[11,12] to express the formulations from $-\infty < M < \infty$,

$$
\begin{array}{l}
C^+ = \alpha_L^+ \left(1+\beta_L\right) M_L - \beta_L M_L^+ - M_{\frac{1}{2}}^+, \quad C^- = \alpha_R^- \left(1+\beta_R\right) M_R - \beta_R M_R^- + M_{\frac{1}{2}}^-, \\
M_L = \frac{U_L}{C_{\frac{1}{2}}}, \quad M_R = \frac{U_R}{C_{\frac{1}{2}}}, \quad \alpha_{L,R} = \frac{1}{2}\left[1 \pm sign\left(M_{L,R}\right)\right], \quad \beta_{L,R} = -max\left[0, 1 - int\left(\left|M_{L,R}\right|\right)\right], \\
M_{\frac{1}{2}}^+ = M_{\frac{1}{2}} \frac{C_R + C_L \Phi}{C_R + C_L}, \quad M_{\frac{1}{2}}^- = M_{\frac{1}{2}} \frac{C_L + C_R \Phi^{-1}}{C_R + C_L}, \quad \Phi = \frac{\left(\rho C^2\right)_R}{\left(\rho C^2\right)_L}, \quad M_{\frac{1}{2}} = \beta_L \delta^+ M_L^- - \beta_R \delta^- M_R^+, \\
M_{L,R}^{\pm} = \pm\frac{1}{4}\left(M_{L,R} \pm 1\right)^2, \quad \text{and} \quad \delta^{\pm} = \frac{1}{2}\left\{1 \pm sign\left[\frac{1}{2}\left(M_L + M_R\right)\right]\right\}.
\end{array}
\tag{47}
$$

The pressure flux, E^p is evaluated as

$$
E_{\frac{1}{2}}^p = \begin{pmatrix} 0 \\ p\, l_x \\ p\, l_y \\ p\, l_z \\ p\overline{U} \end{pmatrix} = \begin{pmatrix} 0 \\ \left(\mathcal{D}_L^+ p_L + \mathcal{D}_R^- p_R\right) l_x \\ \left(\mathcal{D}_L^+ p_L + \mathcal{D}_R^- p_R\right) l_y \\ \left(\mathcal{D}_L^+ p_L + \mathcal{D}_R^- p_R\right) l_z \\ \overline{C}_{\frac{1}{2}} \left(\mathcal{S}_L^+ p_L + \mathcal{S}_R^- p_R\right) \end{pmatrix},
\tag{48}
$$

where,

$$
\mathcal{D}^{\pm}{}_{L,R} = \left[\alpha\left(1+\beta\right) - \beta\mathcal{P}^{\pm}\right]_{L,R}.
\tag{49}
$$

The pressure splitting coefficient is:

$$
\mathcal{P}_{L,R}^{\pm} = \frac{1}{4}\left(M_{L,R} \pm 1\right)^2 \left(2 \mp M_{L,R}\right).
\tag{50}
$$

For the pressure term in the energy equation, the contravariant speed of sound $\overline{C}$ is consistent with $\overline{U}$ and is calculated as:

$$
\overline{C} = C - l_t, \quad \text{with} \quad \mathcal{S}^{\pm}{}_{L,R} = \left[\bar{\alpha}^{\pm}\left(1+\bar{\beta}\right) M - \bar{\beta}\bar{M}\right]_{L,R}, \quad \text{and where} \quad \bar{M} = \frac{\overline{U}}{\overline{C}}.
\tag{51}
$$

$\bar{\alpha}$ and $\bar{\beta}$ are evaluated based on $\bar{M}$ using the formulations given in Eq. (47). The use of $\overline{U}$, $\overline{C}$ and $\bar{M}$ in the pressure term for the energy equation is to take into account the grid speed so that the flux will transit from subsonic to supersonic smoothly. When the grid is stationary, $l_t = 0$, $\overline{C} = C$, $\overline{U} = U$.

The LDE scheme can accurately resolve wall boundary layer profiles, capture crisp shock profiles and exact contact surfaces[10] with low diffusion.

V.B. The Weighted Essentially Non-oscillatory (WENO) Scheme[13]

The fifth-order accurate WENO ($r = 3$) reconstruction of u^L and u^R can be written as

$$
u_{i+1/2}^L = \omega_0 q_0 + \omega_1 q_1 + \omega_2 q_2
$$

where

$$
q_0 = \frac{1}{3}u_{i-2} - \frac{7}{6}u_{i-1} + \frac{11}{6}u_i, \quad q_1 = -\frac{1}{6}u_{i-1} + \frac{5}{6}u_i + \frac{1}{3}u_{i+1}, \quad q_2 = \frac{1}{3}u_i + \frac{5}{6}u_{i+1} - \frac{1}{6}u_{i+2}
$$

with

$$
\omega_s = \frac{\alpha_s}{\alpha_0 + \cdots + \alpha_{r-1}}, \quad \alpha_s = \frac{C_s}{\varepsilon + IS_s}, \quad k = 0, \cdots, r-1, \quad C_0 = 0.1, \quad C_1 = 0.6, \quad \text{and} \quad C_2 = 0.3,
$$

and

$$
\begin{aligned}
IS_0 &= \frac{13}{12}(u_{i-2} - 2u_{i-1} + u_i)^2 + \frac{1}{4}(u_{i-2} - 4u_{i-1} + 3u_i)^2 \\
IS_1 &= \frac{13}{12}(u_{i-1} - 2u_i + u_{i+1})^2 + \frac{1}{4}(u_{i-1} - 4u_i + 3u_{i+1})^2 \\
IS_2 &= \frac{13}{12}(u_i - 2u_{i+1} + u_{i+2})^2 + \frac{1}{4}(u_i - 4u_{i+1} + 3u_{i+2})^2
\end{aligned}
$$

where, $\varepsilon = 10^{-2}$ is used following the recommendation in Shen, Wang, and Zha.[14] The u^R is reconstructed following the symmetry rule as that to the u^L at interface $i + 1/2$. In this paper, the WENO scheme described above is used to evaluate the conservative variables with 5th order accuracy. The interface flux is then approximated with 5th order accuracy based on the approximate Riemann solver of the Roe scheme and the LED scheme based on:

$$E_{i+\frac{1}{2}} = E(Q^L_{i+\frac{1}{2}}, Q^R_{i+\frac{1}{2}}) \tag{52}$$

V.C. Implicit Time Integration

In the current work, the finite difference method is used to discretize the governing equations for a steady state solution. To achieve a high convergence rate, the implicit time marching scheme is used with the unfactored Gauss-Seidel line relaxation. To enhance diagonal dominance, the first order Euler method is used to discretize the temporal term

$$\begin{aligned} &\tfrac{\Delta V}{\Delta t}\left(Q^{n+1} - Q^n\right) + \left(E_{i+\frac{1}{2}} - E_{i-\frac{1}{2}}\right)^{n+1} + \left(F_{j+\frac{1}{2}} - F_{j-\frac{1}{2}}\right)^{n+1} + \left(G_{k+\frac{1}{2}} - G_{k-\frac{1}{2}}\right)^{n+1} \\ &= \tfrac{1}{Re}\left[\left(R_{i+\frac{1}{2}} - R_{i-\frac{1}{2}}\right)^{n+1} + \left(S_{j+\frac{1}{2}} - S_{j-\frac{1}{2}}\right)^{n+1} + \left(T_{k+\frac{1}{2}} - T_{k-\frac{1}{2}}\right)^{n+1} + D^n \Delta V\right] + S^n_{MHD}\Delta V. \end{aligned} \tag{53}$$

where n and $n+1$ are two sequential time levels with a time interval of Δt. A first-order Taylor expansion for the $n+1$ time level is used for all inviscid and viscous terms above. The discretized equations are given as the following

$$\begin{aligned} &\Delta Q^{n+1}_{i,j,k} + A^+\Delta Q^{n+1}_{i+1,j,k} + A\Delta Q^{n+1}_{i,j,k} + A^-\Delta Q^{n+1}_{i-1,j,k} + B^+\Delta Q^{n+1}_{i,j+1,k} + B\Delta Q^{n+1}_{i,j,k} \\ &+B^-\Delta Q^{n+1}_{i,j-1,k} + C^+\Delta Q^{n+1}_{i,j,k+1} + C\Delta Q^{n+1}_{i,j,k} + C^-\Delta Q^{n+1}_{i,j,k-1} = RHS^n, \end{aligned} \tag{54}$$

where RHS^n is the summation of all the terms on the right hand side (RHS) of the equation, and

$$\begin{aligned} RHS^n = \tfrac{\Delta t}{Re\Delta V}\Big\{&\Big[\left(R^n_{i+\frac{1}{2}} - R^n_{i-\frac{1}{2}}\right) + \left(S^n_{j+\frac{1}{2}} - S^n_{j-\frac{1}{2}}\right) + \left(T^n_{k+\frac{1}{2}} - T^n_{k-\frac{1}{2}}\right)\Big] \\ &- \Big[\left(E^n_{i+\frac{1}{2}} - E^n_{i-\frac{1}{2}}\right) + \left(F^n_{j+\frac{1}{2}} - F^n_{j-\frac{1}{2}}\right) + \left(G^n_{k+\frac{1}{2}} - G^n_{k-\frac{1}{2}}\right)\Big]\Big\} + \tfrac{1}{Re}D^n\Delta t + S^n_{MHD}\Delta t. \end{aligned} \tag{55}$$

The Gauss-Seidel line relaxation is applied on each direction respectively and is swept forward and backward once within each physical time. For example, if the sweeping is in the i direction from smaller index to larger one, Eq. [54] will be

$$B^-\Delta Q^{n+1}_{i,j-1,k} + \bar{B}\Delta Q^{n+1}_{i,j,k} + B^+\Delta Q^{n+1}_{i,j+1,k} = RHS' \tag{56}$$

where, $\bar{B} = I + A + B + C$. The terms in the neighboring cells in the i and k directions are absorbed into RHS^n as RHS',

$$RHS' = RHS^n - A^+\Delta Q^n_{i+1,j,k} - A^-\Delta Q^{n+1}_{i-1,j,k} - C^+\Delta Q^n_{i,j,k+1} - C^-\Delta Q^{n+1}_{i,j,k-1} \tag{57}$$

The unfactored implicit Gauss-Seidel line relaxation employed in this paper is significantly more efficient than the LU-SGS implicit scheme.[15]

VI. Validation of Code

For validation purposes we plot curves in Fig. [1] (all the figures are at the end of the paper) that show excellent agreement between the result of our code and the numerical integration of the exact self-similar solution of the Blasius problem of compressible viscous flow over a flat adiabatic plate at Mach 2. The temperature boundary condition at the plate is $dT/dy = 0$. In the figures the eta on the vertical axis is

$$\eta = y\sqrt{\frac{U_\infty}{\nu x}} = \frac{y}{x}\sqrt{R_{e_x}}. \tag{58}$$

VII. Mach 5 MHD Flow With Turbulence Over a Flat Plate

We apply the above numerical method to the problem same problem as in Khan[9] of two-dimensional hypersonic flow in the $x-y$ plane, with $\mathbf{u} = u\hat{\mathbf{x}} + v\hat{\mathbf{y}}$, at zero angle of attack past a 1 m long flat plate that lies on the $x-z$ plane. The computational region is 1.6 m tall in the y direction. The computational mesh is shown in Fig. [2]. The z coordinate is ignorable, so $\partial/\partial z = 0$ for all quantities. We take the electric field to be zero, and we apply a uniform magnetic field in the y direction $\mathbf{B}_a = B_a\hat{\mathbf{y}}$ as in Refs. [6] and [9]. There is no transformation to the ξ, η, ζ variables, so $\mathbf{l} = \hat{\mathbf{x}}$, and $\mathbf{m} = \hat{\mathbf{y}}$. On the surface of the body we use the adiabatic boundary condition $\partial T/\partial y = 0$, for the temperature, and the no slip condition $u = 0$ for the velocity. We use the Sutherland model for viscosity with $\mu_\infty = 1.69 \times 10^{-5}$ Pa·s, and the Baldwin-Lomax turbulence model. We use a molecular Prandtl number of 0.72, and a turbulent Prandtl number of 0.9. Our time marching solution uses a uniform velocity profile for the initial velocity field. We take the electrical conductivity to be uniform throughout the computational region with a value of $\sigma = 100$ S/m. This is a the low end of the range of values found for the conductivity in the work of Yoshino, Fujino, and Ishikawa,[16] where they find the σ can go as high as 700 S/m in the hottest regions. We use conditions at an altitude of about 45 km, where the ambient pressure is $p_\infty = 143$ Pa, the air density is $\rho_\infty = 1.88 \times 10^{-3}$ kg/m^3, the ambient temperature is $T_\infty = 265$ K, and the speed of sound is 331 m/s. The total temperature T_t at the inlet computational boundary is

$$T_t = T\big(1 + \frac{\gamma - 1}{2}M^2\big) = 6T = 6 \times 265K = 1590K. \tag{59}$$

The incoming flow has Mach number $M_\infty = 5$. The Reynolds number of 1.84×10^5 is based on a characteristic length of 1 m. The magnetic Reynolds number is $R_m = 0.208$. Fig. [3] shows our results for a plot of the dimensionless velocity $u(x = 0.9\,\mathrm{m}, y)/U_\infty$ for $0 \le y \le 0.1$ m with applied magnetic fields B_a varying from 0 T to 0.02 T. The numerical scheme used is indicated at the top of all the figures. The curves show the trend that $u(x = 0.9\,\mathrm{m}, y)$ decreases slightly for moderate values of B_a. This is as it should be since the magnetic force $\mathbf{J} \times \mathbf{B}$ opposes the fluid velocity. Fig. [4] shows a plot of the dimensionless temperature $T(x = 0.9\,\mathrm{m}, y)/T_\infty$ for $0 \le y \le 0.1$ m. The curves show the trend that $T(x = 0.9\,\mathrm{m}, y)$ increases slightly as B_a increases. This should happen because as the fluid is slowed down adiabatically by the magnetic force its temperature should increase. Fig.[5] shows color graphs of pressure and temperature fields as the applied magnetic field increases from 0 T to 500 Gauss. The x and y axes are labeled in meters. The effect of the magnetic field on the pressure in the left panel becomes very pronounced at 0.05 T. In the right panel we see how the temperature increases as the magnetic field slows down the flow adiabatically. The temperature increase occurs over a much larger region when the magnetic field reaches 0.05 T.

VIII. Mach 10 Laminar MHD Flow Around an Insulated Blunt Body

Here we consider laminar hypersonic flow over a blunt body with Mach number $M_\infty = 10$. The computational grid is shown in Fig. [6]. On the surface of the body we again use the adiabatic and no slip boundary conditions $\hat{\mathbf{n}} \cdot \vec{\nabla} T = 0$, and $\mathbf{u} = 0$, where $\hat{\mathbf{n}}$ is a unit vector normal to the body surface, and $\mathbf{u}$ is the fluid velocity at the surface of the body. We use the same Prandtl numbers as above and we again use the Sutherland model for viscosity, but with $\mu_\infty = 1.5 \times 10^{-5}$ Pa·s. Our time marching solution again uses a uniform flow for the initial velocity field. Here we use air properties at a height of 70 km. We take an ambient pressure of $p_\infty = 4.63$ Pa, an air density of $\rho_\infty = 7.08 \times 10^{-5}$ kg/m^3, an ambient temperature of $T_\infty = 228$ K, and a speed of sound of 302 m/s. The parameters are similar to those in Ref. [6] except that the Reynolds number, which is based on a characteristic length of 0.14 m, is $R_e = 2 \times 10^3$ corresponding to an altitude of 70 km. The molecular Prandtl number is taken as 0.72. We take the electrical conductivity to be uniform throughout the computational region, but we consider simulations with values that range from $\sigma = 100$ S/m to 300 S/m. Fig. [7] shows the pressure and temperature fields with $\sigma = 100$ S/m for applied magnetic fields of $B_y = 0$, $B_y = 0.05$ T, and $B_y = 0.1$ T. With $\sigma = 100$ S/m the magnetic Reynolds number is $R_m = 0.0531$. The left panel shows that the magnetic field has moved the shock farther away from the body and the isobars are also moved farther from the body. The yellow regions in the right panel show a general temperature increase behind the shock as we increase the magnetic field. The same effects are seen in Fig. [8] as σ increases from 100 to 300 S/m, but more strongly because of the higher electrical conductivity.

IX. Future Work

We are working on improving our simulations to deal with three dimensional flows, stronger magnetic fields and higher Mach numbers. We will also put turbulence into the blunt body flows using the Baldwin - Lomax turbulence model and the (S-A) one equation turbulence model.

Acknowledgments

This work was supported in part by the U. S. Air Force Office of Scientific Research under Grants FA9550-06-1-0002 monitored by Dr. Robert Barker, and FA49620-03-1-0253 monitored by Dr.Fariba Fahroo. We also acknowledge the valuable assistance of Dr. Zha's student, Mr.Baoyuan Wang.

References

[1]Bityurin, V. A., Lineberry, J. T., Potebnia, V. G., Alferov, V. I., Kuranov, A. L., and Sheikin, E. G., "Assessment of Hypersonic MHD Concepts," AIAA Paper 97-2393, 1997.

[2]Bityurin, V. A. and Bocharov, A. N., "Effects of MHD Interaction in Reentry Flight," AIAA Paper 2006-3235, 2006.

[3]Zeigarnik, V. A. B. V. A., , and Kuranov, A. L., "On a Perspective of MHD Technology in Aerospace Applications," AIAA Paper 1996-2355, 1996.

[4]Fujino, T., Kon, S., and Ishikawa, M., "Preliminary Analysis of Electric Power Extraction by MHD Technology in Reentry Flight," AIAA Paper 2007-4248, 2007.

[5]MacCormack, R. W., "Simulation of Hypersonic Flow within a Strong Magnetic Field," AIAA Paper 2007-397, 2007.

[6]Hoffmann, K. A., Damevin, H. M., and Dietiker, J., "Numerical Simulation of Hypersonic NUumber Magnetofluiddynamic Flows," AIAA Paper 2000-2259, 2000.

[7]MacCormack, R. W., "Flow Simulations within Strong Magnetic Fields," AIAA Paper 2008-1070, 2008.

[8]*Numerical Simulations of Hypersonic Magnetogasdynamic Flows Over Blunt Bodies*, 2002.

[9]Khan, O. U., Hoffmann, K. A., and Dietiker, J., "Validity of Low Magnetic Reynolds NUumber Formulation of Magnetofluiddynamics," AIAA Paper 2007-4374, 2007.

[10]Zha, G.-C., Shen, Y., and Wang, B., "Calculation of Transonic Flows Using WENO Method with a Low Diffusion E-CUSP Upwind Scheme," AIAA Paper 2008-0745, 46th AIAA Aerospace Sciences Meeting, Reno, NV, Jan. 2008.

[11]Edwards, J. R., "A Low-Diffusion Flux-Splitting Scheme for Navier-Stokes Calculations," AIAA Paper 95-1703-CP, June, 1995.

[12]Edwards, J. R., "A Low-Diffusion Flux-Splitting Scheme for Navier-Stokes Calculations," *Computer & Fluids*, Vol. 6, 1997, pp. 635–659.

[13]Shu, C.-W., "Essentially Non-Oscillatory and Weighted Essentially Non-Oscillatory Schemes for Hyperbolic Conservation Laws," NASA /CR-97-206253, ICASE Report NO.97-65, 1997.

[14]Shen, Y.-Q., Wang, B.-Y., and Zha, G.-C., "Applications of Implicit WENO Scheme for Compressible Flows ," AIAA Paper 2007-4431, 2007.

[15]Shen, Y.-Q. and Zha, G.-C., "A Comparison Study of Gauss-Seidel Iteration Methods for Internal and External Flows," AIAA Paper 2007-4332, 2007.

[16]Yoshino, T., Fujino, T., and Ishikawa, M., "Numerical Analysis of Rentry Trajectory Coupled with MHD Flow Control," AIAA Paper 2007-4249, 2007.

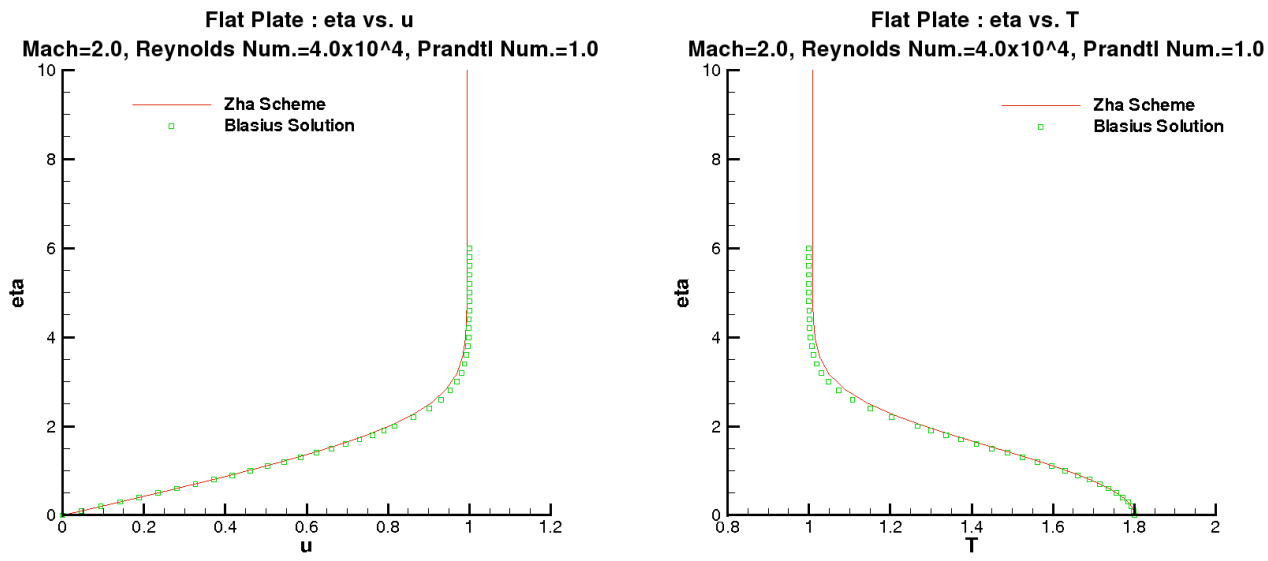

Figure 1. u/U_∞ and T/T_∞ obtained from E-CUSP code compared with Blasius solution for Mach 2

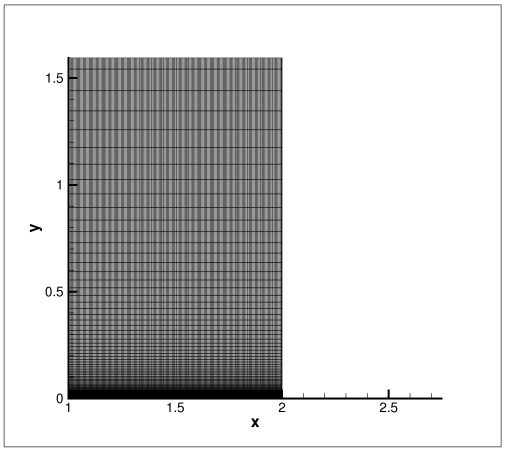

Figure 2. Computational grid for the 1 meter long flat plate.

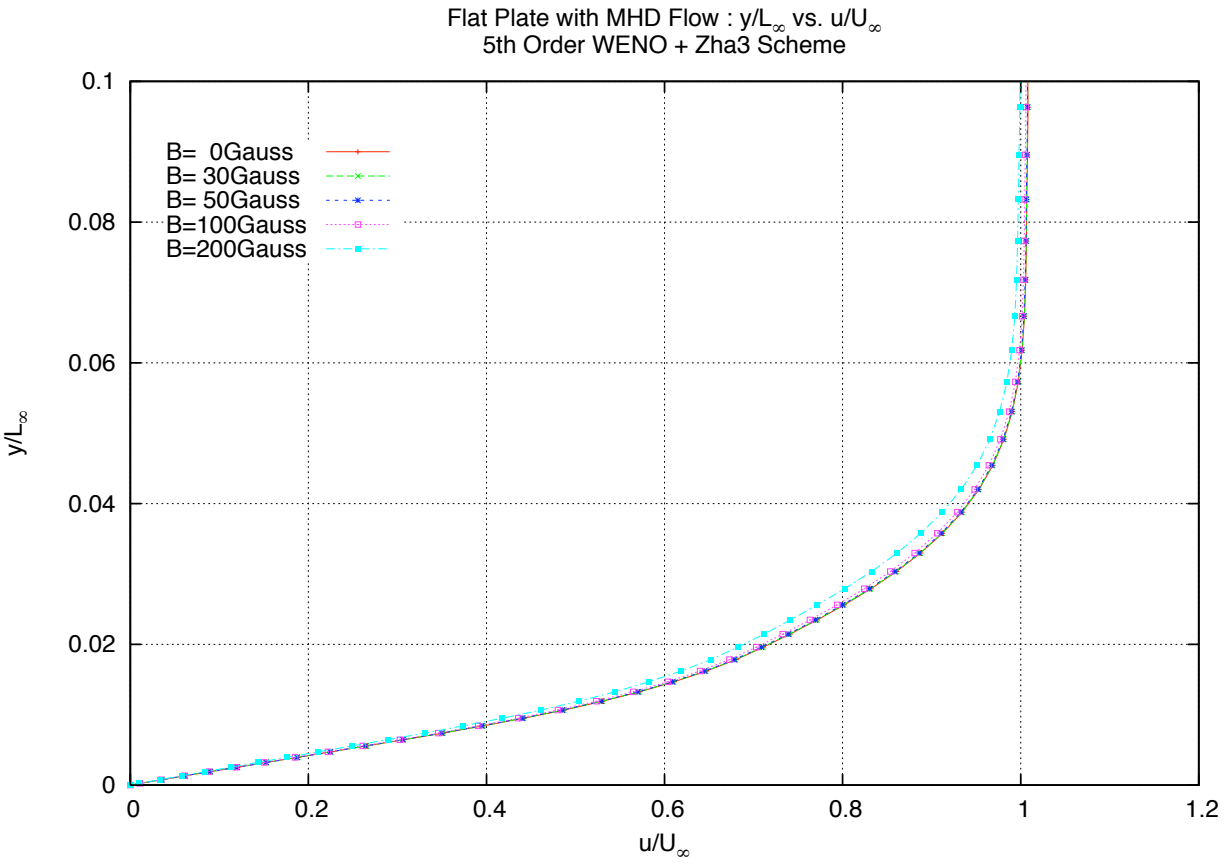

Figure 3. Dimensionless velocity u/U_∞ as a function of y at fixed $x \approx 0.9$ m for different values of the magnetic field.

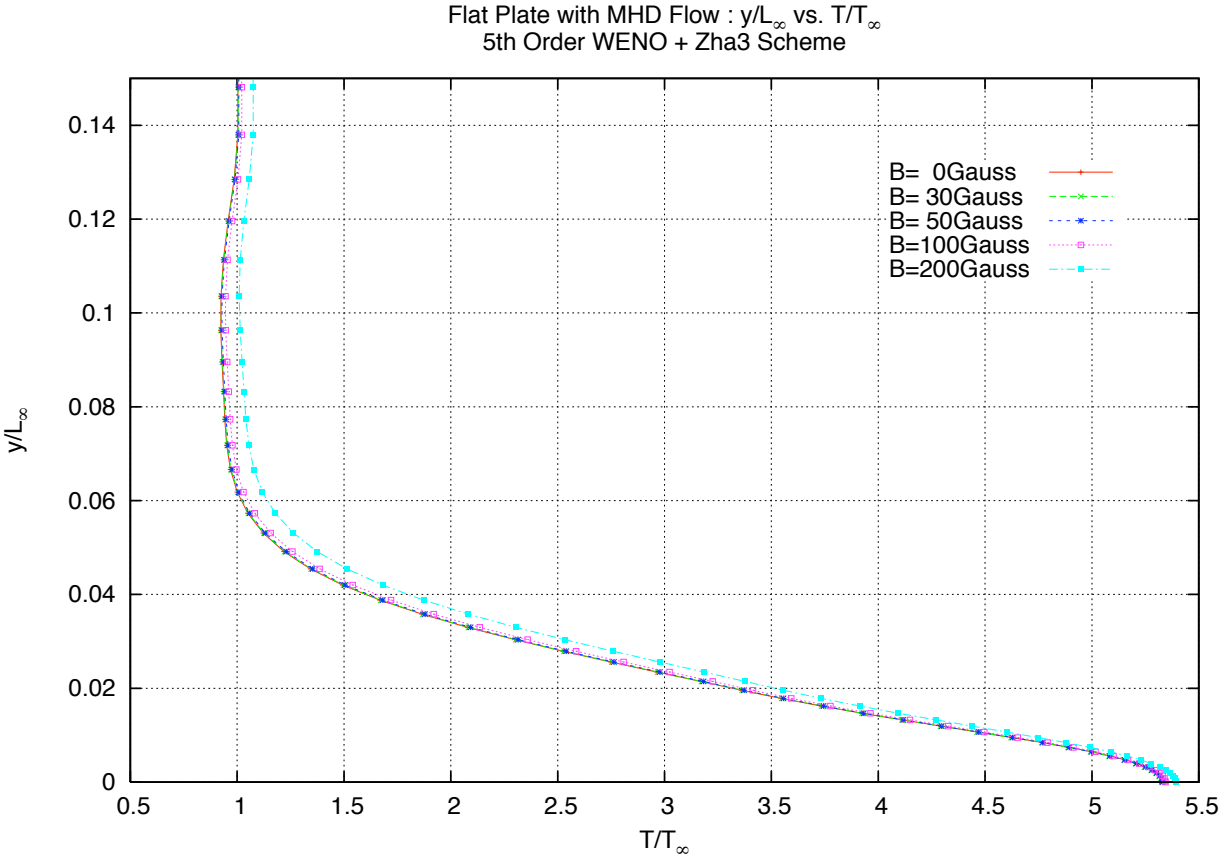

Figure 4. Dimensionless temperature T/T_∞ at $x \approx 0.9$ m for different values of the magnetic field.

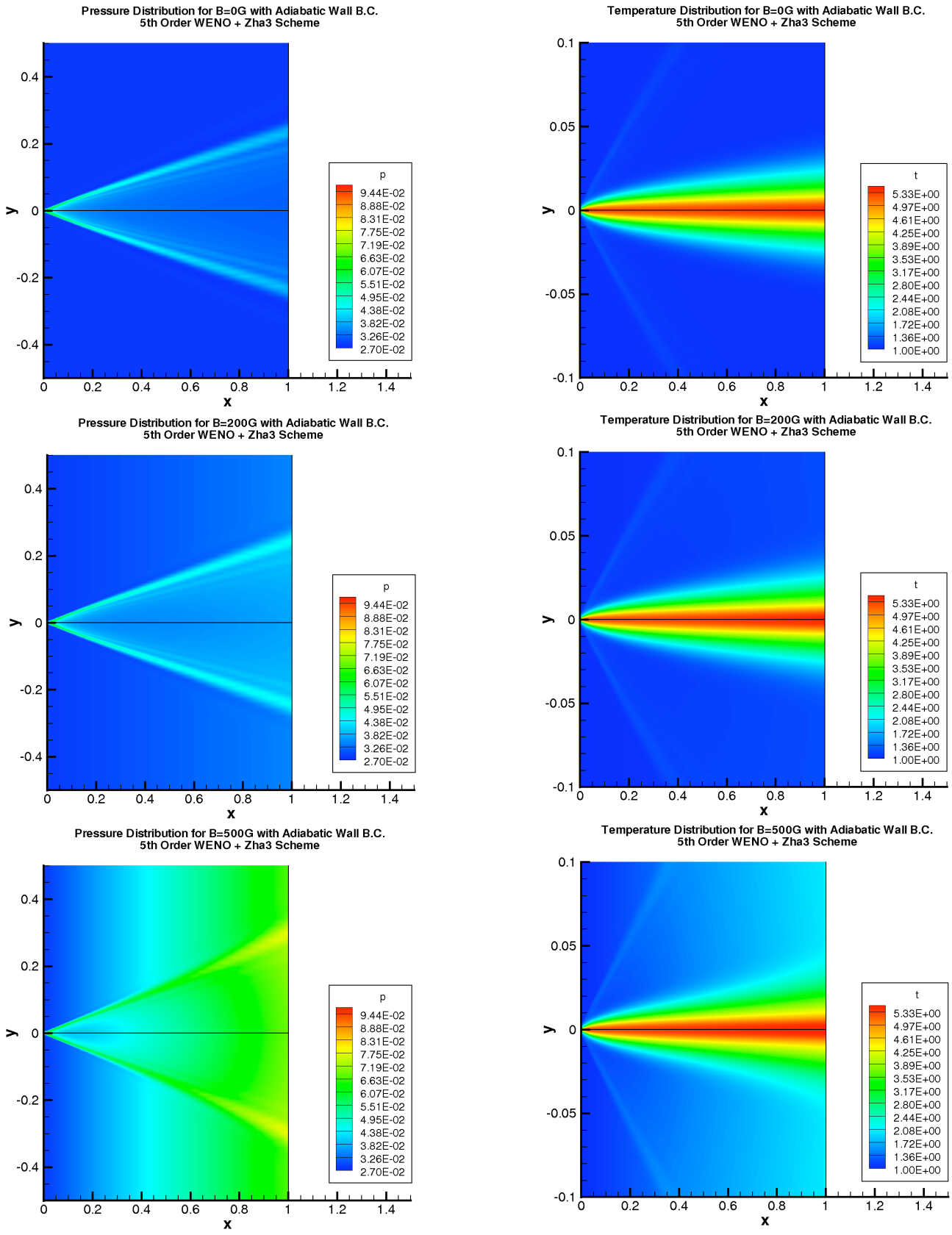

Figure 5. Temperature and pressure fields with $\sigma = 100$ S/m for magnetic fields of 0, 30, and 50 Gauss.

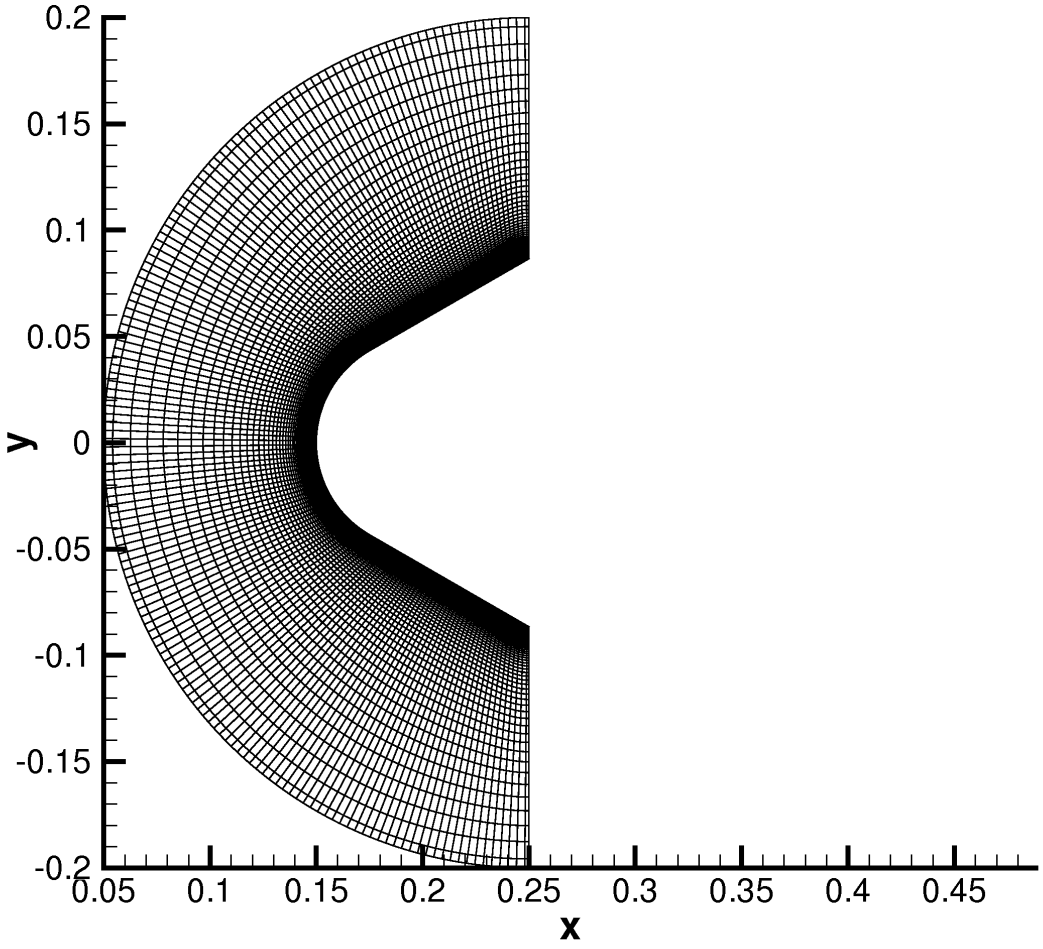

Figure 6. Computational grid for flow around a blunt body. The tick marks on the axes are in meters.

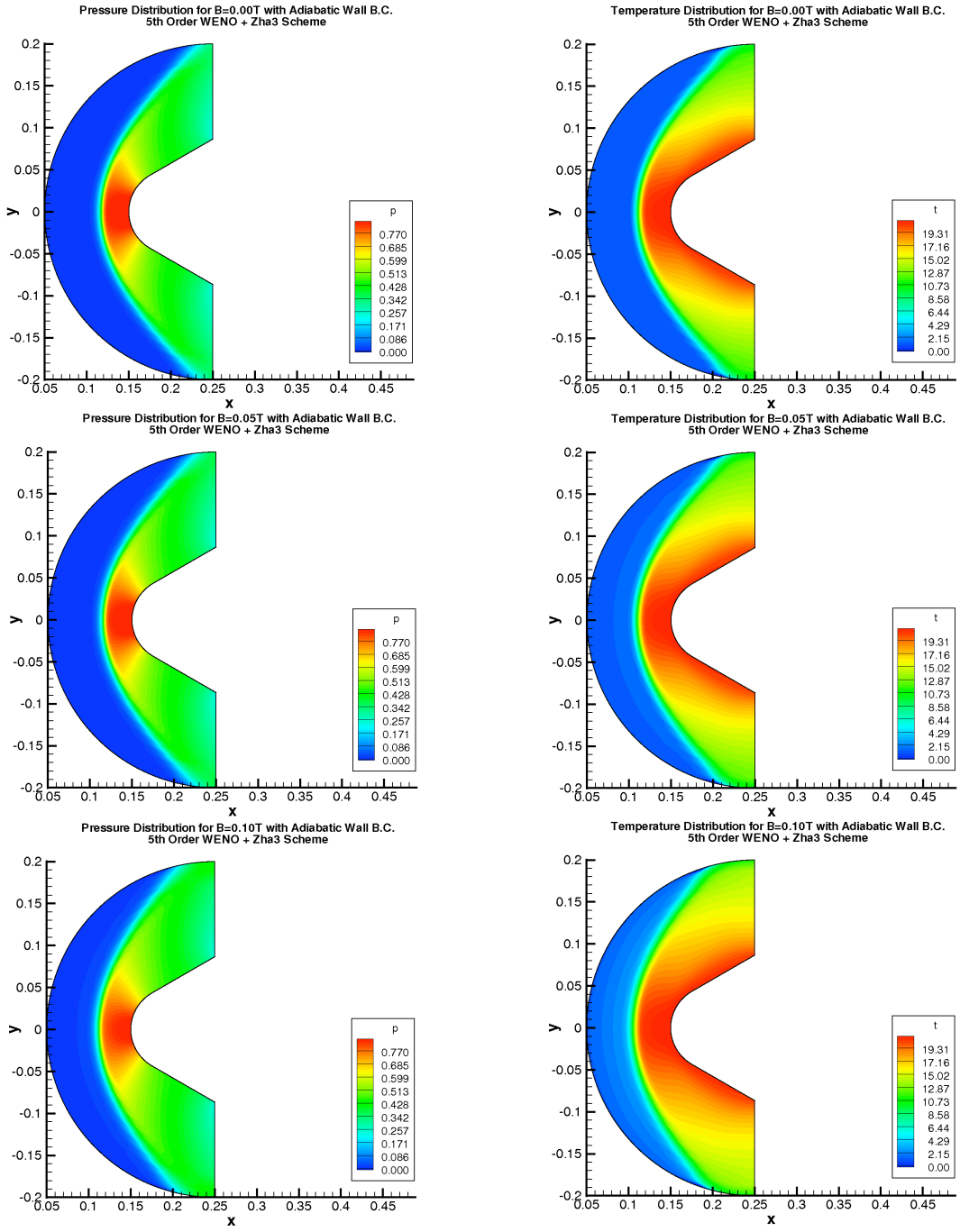

Figure 7. Pressure and temperature fields with $\sigma = 100$ S/m for magnetic fields of 0 T, 0.05 T, and 0.1 T

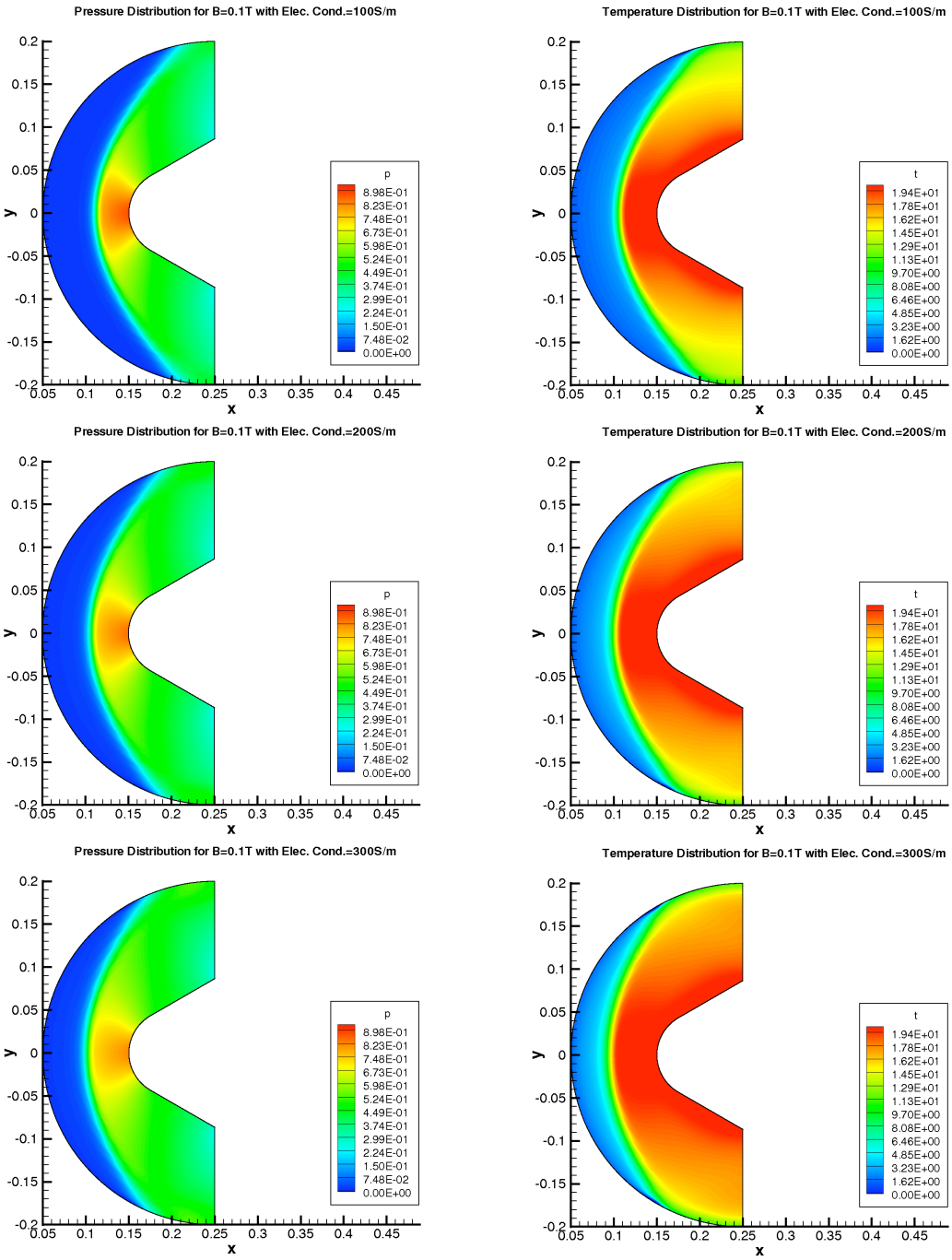

Figure 8. Pressure and temperature fields with constant $B_y = 0.1T$ electrical conductivity values of 100, 200, and 300 S/m.